Chemical Engineering Journal 507 (2025) 160622

Contents lists available at ScienceDirect

Chemical Engineering Journal

journal homepage: www.elsevier.com/locate/cej

Catalytic conversion of paper sludge carbohydrates to jet fuel range hydrocarbons: Process optimization and techno-economic analysis

David Cruz [a], Hyeonji Park [a], Phoenix Tiller [a], Adarsh Kumar [b], Ronalds Gonzalez [a], Ashutosh Mittal [b], David K. Johnson [b], Sunkyu Park [a,*]

[a] Department of Forest Biomaterials, North Carolina State University, Raleigh, NC 27695, USA
[b] Renewable Resources and Enabling Sciences Center, National Renewable Energy Laboratory, Golden, CO 80401, USA

ARTICLE INFO

Keywords:
Biorefinery
Bioeconomy
Process design
Waste valorization
Pulp and paper
Solvent analysis

ABSTRACT

This study presents a catalytic pathway involving seven pretreatment and conversion steps to upgrade carbohydrates in paper sludge into a hydrocarbon blend compatible with conventional aviation fuel. Fuel-critical properties analysis by two independent laboratories confirmed that 44.3 % of the resulting hydrocarbon product meets Jet A standards. Nine biorefinery configurations were examined to identify strategies for reducing the minimum fuel selling price (MFSP) of the final hydrocarbon product. Techno-economic analysis revealed that replacing 1,4-dioxane with acetone and increasing sugar concentration during the dehydration step, along with using biobased methyl ethyl ketone in aldol-condensation, are key factors in reducing the MFSP from $8.6 per gasoline gallon equivalent (GGE) in the base case to $4.5/GGE in the optimized scenario. A sensitivity assessment was conducted for each configuration analyzed to identify additional process optimization opportunities to enhance the economic viability of the biorefinery process relative to conventional jet fuel.

1. Introduction

The rising global population and anticipated higher living standards will result in an expanded demand for energy and products and an increase in anthropogenic carbon dioxide emissions that exceed the natural absorption capacity of biological and geological carbon cycles [1,2]. Fossil fuels supply most of the world's energy demand, and the transportation sector predominantly relies on the existing reserves of these non-renewable resources [3]. To mitigate the risks associated with fossil fuel depletion, producing transport fuels from renewable sources has gained interest from both the scientific community and oil and gas companies [4,5]. Recent energy demand projections indicate that high-energy–density liquid fuels will remain essential for the heavy transportation sector, including marine transport and long-distance aviation. This need arises from the current limitations of the commercially available low-energy–density battery technologies and the high costs associated with transitioning to hydrogen fuel cells [5,6].

In the United States, the transportation sector is the most significant contributor to anthropogenic greenhouse gas (GHG) emissions. In 2022, this economic sector contributed 28.5 % (1,808 million metric tons of CO_2 Equivalent) of the total U.S. GHG emissions, with air transport −including commercial, military, and general aviation- contributing 2.0 % of the total U.S. GHG emissions in the same year [7,8]. To reduce aviation GHG emissions, the U.S. government has outlined The Sustainable Aviation Fuel (SAF) Grand Challenge as a strategy to advance the aviation industry by supporting innovation and leading progress to achieve the goal of net-zero GHG by 2050. This effort, led by several federal agencies (DOE, DOT, USDA, etc.,), aims to integrate new aircraft technologies, operational improvement strategies, and expand SAF domestic consumption to 3 billion gallons per year by 2030, and 35 billion gallons to cover 100 % of the aviation fuel consumption projected in 2050 [9,10]. SAF is an alternative advanced fuel under the Renewable Fuel Standard program (RFS) produced from non-petroleum sources, such as biomass and waste, that reduces emissions from the air transportation sector [11]. The SAF Grand Challenge requires fuels to reduce emissions by at least 50 % on a life-cycle assessment basis compared to conventional jet fuel [12]. Depending on the production pathway and the source of carbon backbone, this drop-in fuel can be blended with

* Corresponding author at: North Carolina State University, Department of Forest Biomaterials, NC State University, Biltmore Hall, Campus Box 8005, Raleigh, NC 27695-8005 USA.
E-mail addresses: cdcruzri@ncsu.edu (D. Cruz), hpark22@ncsu.edu (H. Park), pstiller@ncsu.edu (P. Tiller), adarsh.Kumar@nrel.gov (A. Kumar), rwgonzal@ncsu.edu (R. Gonzalez), ashutosh.mittal@nrel.gov (A. Mittal), david.johnson@nrel.gov (D.K. Johnson), sunkyu_park@ncsu.edu (S. Park).

https://doi.org/10.1016/j.cej.2025.160622
Received 16 November 2024; Received in revised form 3 February 2025; Accepted 12 February 2025
Available online 15 February 2025

conventional Jet A with limits between 5 % and 50 % [13,14]. In all cases, SAF must meet ASTM D7566 standard specifications for aviation turbine fuel containing synthesized hydrocarbons, and ASTM D1655 standard specification for aviation turbine fuels, before blending (ASTM-certified).

The global commercial jet fuel market, currently at 106 billion gallons annually, is expected to surpass 230 billion gallons by 2050 [15]. In the U.S. alone, only 15.8 million gallons of SAF were produced in 2022, less than 0.1 percent of the 17.5 billion gallons of jet fuel consumed by major U.S. airlines that year. This falls significantly short of the Federal Aviation Administration's target for U.S. airlines to use 1 billion gallons of SAF annually by 2018 [16]. Considering the growing potential of the emerging SAF market and the opportunity to become a leading exporter of both technology and fuel, becoming a global leader in developing new technologies for SAF production is crucial for the U.S. economy [12].

Liquid transportation fuels, including drop-in aviation fuel, can potentially be produced from lignocellulosic biomass via different thermochemical and biochemical conversion pathways [17,18]. The major constituents of this abundant second-generation feedstock are cellulose (30 %-50 %), hemicellulose (20 %-40 %), and lignin (10 %-45 %) [19]. The catalytic upgrading of furans [20], one of the most studied pathways for transforming lignocellulosic biomass into hydrocarbon products, involves the formation of carbon–carbon bonds after producing intermediate chemicals from the starting C_5-C_6 monosaccharide feedstocks as a strategy to produce alkanes in the C_8-C_{16} jet fuel range [21]. In this alternative pathway, glucose, and xylose are isomerized and dehydrated, frequently over Lewis acid catalysts (e.g., $AlCl_3$, $CrCl_3$, etc.,) in the presence of organic solvents (1,4-dioxane, DMSO, etc.,) to promote high yields of 5-hydroxymethylfurfural (5-HMF) and furfural, two significant building blocks for the production of intermediate chemicals that can potentially replace petroleum-based feedstocks, as highlighted in the Top 10 Value-added Bio-based Chemicals Volume I report by the U.S. Department of Energy [22]. The next step incorporates aldol-condensation, a well-known reaction in synthetic organic chemistry, used to adjust the carbon length in the resulting hydrocarbon product by condensing 5-HMF and furfural with molecules capable of forming carbanion species, such as ketones (e.g., acetone, 2-butanone, etc.,) using sodium hydroxide as a catalyst for the reaction [23]. A single-step aldol-condensation reaction between monomeric sugar-derived furans (5-HMF or furfural) and short carbon chain ketones yield C_8-C_{10} oxygenated monoadduct products. However, aldol-condensation can occur simultaneously at both α-carbons adjacent to the carbonyl group of the ketone molecule, resulting in longer carbon chain diadducts (C_{13}-C_{16+}). Finally, the last conversion step in the furans route includes the saturation of carbon–carbon double bonds, the opening of ring structures, and the removal of oxygen from the aldol-condensation products to produce the final hydrocarbon blend product through heterogeneous catalytic hydrogenation and hydrodeoxygenation at moderate temperatures (300 °C-400 °C), elevated pressure (up to 200 bar), and over supported metals, such as metal oxides (e.g., Pt on γ-Al_2O_3 and SiO_2), metal carbides (e.g., Mo_2C), and metal phosphides (e.g., Ni_2P/SiO_2) [24,25].

In 2023, the U.S. produced 72 million metric tons of paper and paperboard, and 45 million metric tons of wood pulp [26]. The pulp and paper industry is recognized for its efficient process strategies to optimize the use of wood pulping chemicals and for recovering heat and power from the combustion of biogenic carbon. However, during the paper-making process, a fraction of fine lignocellulosic fibers is not retained in the paper web. These fibers, mixed with mineral additives and other materials in the aqueous effluents of paper mills, form a solid waste known as paper sludge [27]. Landfilling is the most prevalent method for disposing of paper sludge. Identifying alternative solutions for managing this heterogeneous material would reduce environmental and financial impacts, while addressing the limitations of landfill site capacity [28]. In 2024, in the U.S., 268 operating sites collectively produce 10,360 air-dried metric tons per day (AD mt/day) of paper sludge, with 30 sites producing more than 100 CE mt/day and 4 producing over 270 CE mt/day [96].

The foremost attempt of the present work is to produce a hydrocarbon blend in the jet-fuel range derived from carbohydrates in paper sludge through a multi-stage catalytic pathway, which has not been widely studied so far to our best understanding. Bench scale optimization experiments and pilot plant scale operations were integrated to generate sufficient hydrocarbon products to perform fuel-critical property tests at two independent laboratories. The optimized experimental results were used to simulate nine biorefinery configurations, incorporating process modifications through Aspen Plus™ (v11) for mass and energy balance evaluation. A techno-economic analysis was conducted for each case studied to estimate the MFSP of the hydrocarbon product. Additionally, a sensitivity assessment was performed on varying process, economic, and financial parameters to evaluate their impact on the MFSP of the hydrocarbon product in each alternative scenario and to identify potential improvement opportunities for future research on hydrocarbon fuel production via the catalytic upgrading of furans.

2. Materials and methods

2.1. Paper sludge characterization

This study used paper sludge from a Kraft pulp mill producing uncoated freesheet. The characterization of this material, including consistency, carbohydrate content, soluble and insoluble lignin content, and ash content, was performed following NREL analytical procedures [29–31].

2.2. Process description

The foundation for the biorefinery process used in this work is derived from the production of hydrocarbon fuels through the catalytic upgrading of furans, as outlined in NREL/TP-5100–80652 [20]. Fig. 1 illustrates the catalytic pathway considered following the enzymatic hydrolysis of deashed paper sludge. The biorefinery is divided into seven areas (A100 to A700), with detailed descriptions provided in Section 3.9 of this document. The flow diagram for the base-case biorefinery producing hydrocarbon products derived from paper sludge is shown in Fig. 2**a**.

2.3. Ash removal

Before chemical transformations are conducted on carbohydrates found in paper sludge, ash must be removed, as it inhibits enzyme activity, as demonstrated in previous work by this research group [32]. To study and identify optimal process conditions for maximizing ash removal and carbohydrate retention, a Pulmac MasterScreen™ lab scale screen (Pulmac Systems International, Inc., USA) with different screen plates, as well as a pilot-scale system featuring a static Sidehill screen model 554–2-285 (28″ x 50″, Sprout-Bauer, Inc / Andritz, Inc., Austria), along with a hydro pulper capable of processing up to 5.0 oven-dry metric tons (OD mt) of paper sludge per day, was employed at the Department of Forest Biomaterials at North Carolina State University (NCSU).

2.4. Enzymatic hydrolysis

A bench-scale study to optimize enzymatic hydrolysis of deashed sludge was conducted using Cellic® Ctec2 (Novozymes, USA) and an incubator shaker (New Brunswick Scientific, USA) at NCSU. To produce sufficient monomeric sugars for further processing, a pilot-scale 30-L paddle-type reactor (Flash Point Equipments Pvt. Ltd., India) with a 2.0 OD kg capacity at 15 % solids, along with Cellic® Ctec3 (Novozymes, USA), was used at NREL's Integrated Biorefinery Research Facility. Hydrochloric acid (Thermo Fisher Scientific, Inc., MA) was used to

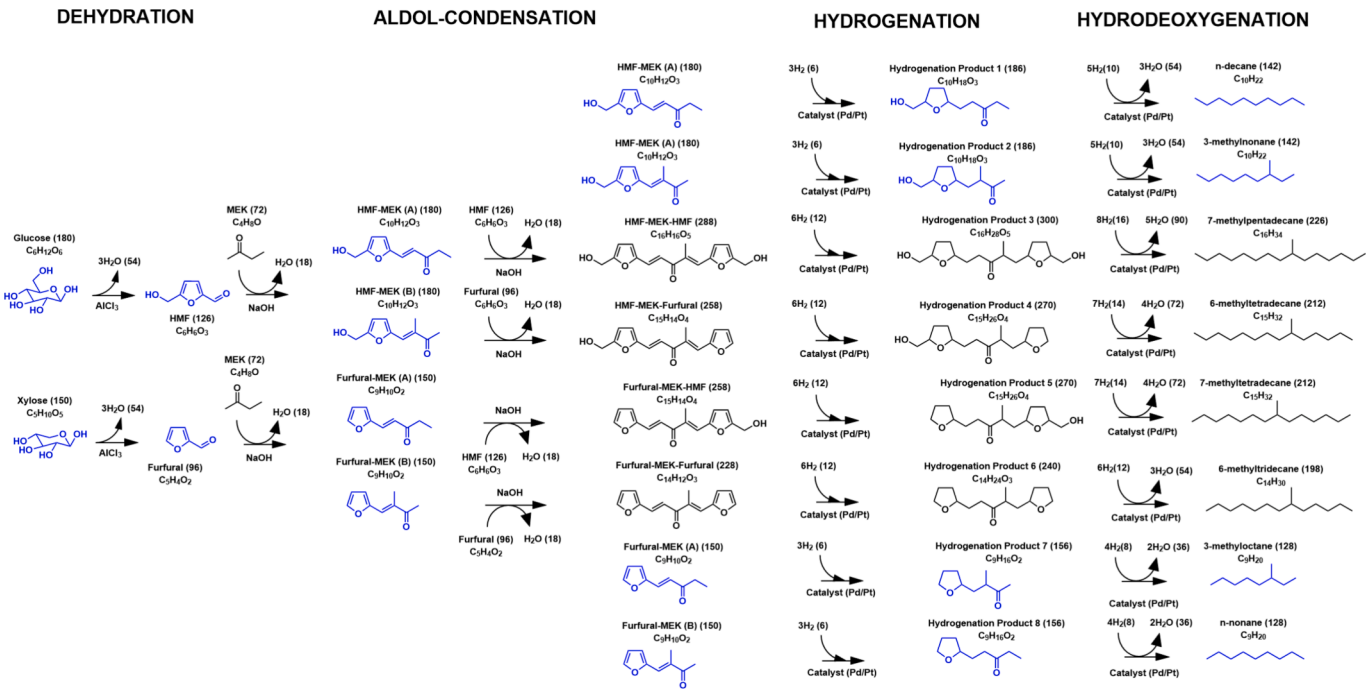

Fig. 1. Catalytic pathway for transforming monomeric sugars derived from carbohydrates in paper sludge into hydrocarbon products. Different monoadducts are produced during the aldol condensation reaction when condensation occurs on the primary or secondary carbon adjacent to the carbonyl group of MEK. Furthermore, homogeneous and heterogeneous diadducts can be formed when aldol-condensation occurs simultaneously at both α-carbons adjacent to the carbonyl group of MEK. The targeted intermediate products for producing C_9 and C_{10} hydrocarbons are highlighted in blue. (For interpretation of the references to colour in this figure legend, the reader is referred to the web version of this article.)

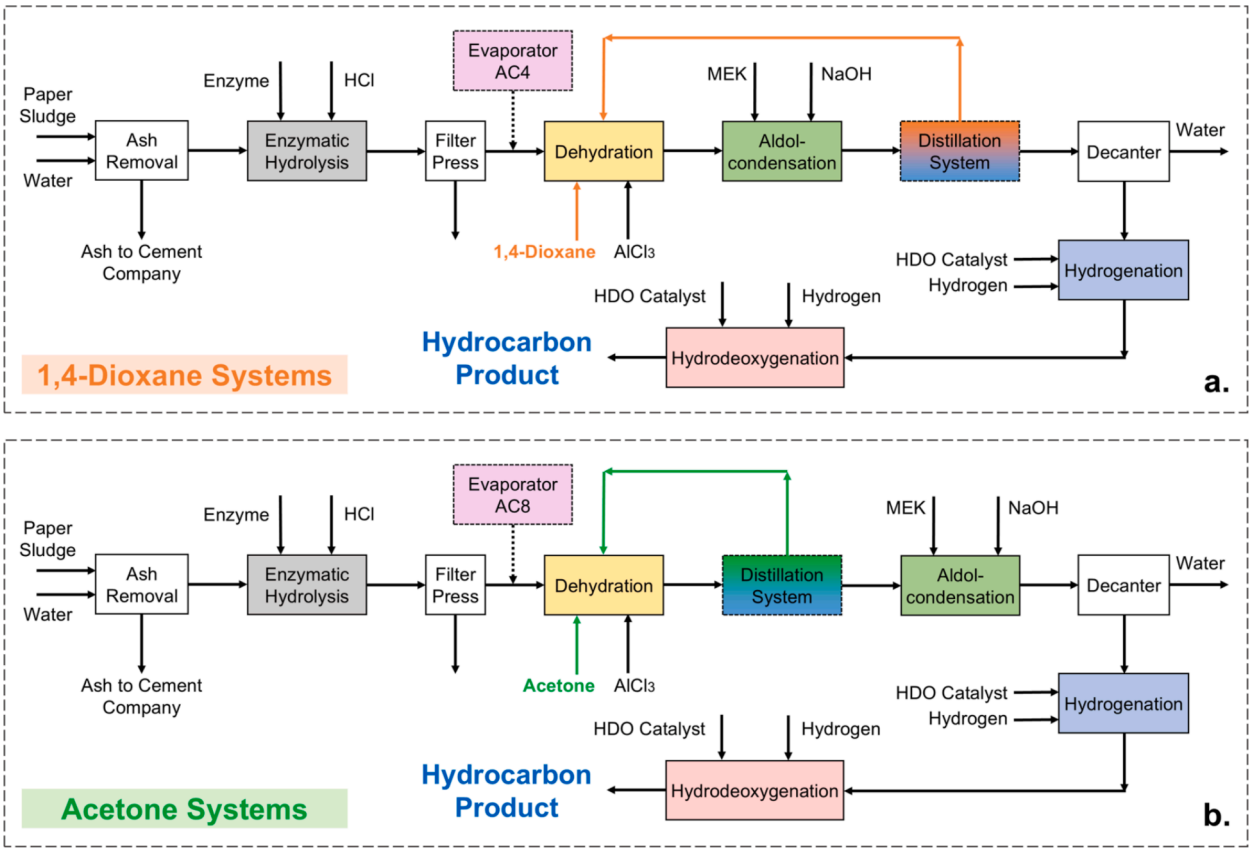

Fig. 2. Flow diagram for biorefineries producing hydrocarbon products derived from carbohydrates in paper sludge, utilizing (a) 1,4-dioxane and (b) acetone as organic solvent during the sugar dehydration reaction, emphasizing the need to relocate the solvent recovery step when acetone is used.

adjust pH for optimal enzyme performance. Sugars were quantified using an Agilent 1200 HPLC system (Agilent Technologies, Inc., USA) with a Refractive Index Detector (RID) and a Shodex SP0810 column (Resonac, Japan) [29].

2.5. Sugar dehydration

A CEM Microwave Synthesizer Discover® 2.0 (CEM Corporation, USA) was used at NCSU to optimize reaction conditions and test alternative organic solvents to maximize the yields of 5-HMF and furfural in the dehydration of sugars derived from hydrolyzed deashed paper sludge. At NREL, a continuous flow reactor with glass-lined tubing (½ inch outer diameter, 0.065-inch wall thickness) and a 25-inch heating zone scaled up the reaction to produce enough 5-HMF and furfural for further chemical steps. Aluminum chloride ($AlCl_3$) (Thermo Fisher Scientific, Inc., MA) served as a Lewis acid catalyst. 5-HMF and furfural were quantified using an Agilent HPLC 1100 system (Agilent Technologies, Inc., USA) with a Waters C18 reversed-phase column (Waters Corporation, USA).[33].

2.6. Solvent recovery

A continuous distillation system with fourteen total equilibrium stages was set up at NCSU to recover the organic solvent used in the dehydration reaction of sugars. The setup included two six-section Snyder columns (ACE Glass, Inc., USA), a 500 ml round-bottom flask, a Graham condenser, a heating mantle with magnetic stirring (Thermofisher Scientific, Inc., USA), two peristaltic pumps (Golander LLC, USA), and two temperature controllers (J-Kem Scientific, Inc., USA).

2.7. Aldol-condensation reaction

Sodium hydroxide (Thermofisher Scientific, Inc., USA) was used as a catalyst for the aldol-condensation reaction between 5-HMF and furfural with MEK. A water bath reactor with twenty-five 10-ml vessels and an IKA C-Mag HS 7 magnetic hotplate stirrer (IKA Works, Inc., USA) was used to optimize conditions for maximizing aldol-condensation yield. For scaling up the reaction, an IKA Eurostar 60 overhead stirrer (IKA Works, Inc., USA), a 5-L heating mantle (Thermofisher Scientific, Inc., USA), and a 5-L round-bottom flask were employed. 2-pentanone (Sigma-Aldrich Corp., USA) was used to extract aldol-condensation products, and magnesium sulfate (Thermofisher Scientific, Ind., USA) was used to dry the extract. An IKA® RV10 rotary evaporator (IKA Works, Inc., USA) was used to remove 2-pentanone. The resulting oxygenated adducts were analyzed using an Agilent 1220 HPLC system with a Variable Wavelength Detector (VWD) and an InfinityLab Poroshell 120 EC-C18 column (Agilent Technologies, Inc., USA).

2.8. Low-temperature hydrogenation and hydrodeoxygenation

A 5000-series Parr multi-reactor system (Parr Instrument Company, USA) was used at NREL for low-temperature hydrogenation and hydrodeoxygenation (HDO) reactions. Supported palladium (Pd) or platinum (Pt) catalysts (5 % metal), impregnated onto a SiO2-Al2O3 support (GRACE Davicat® SIAL 3115, ~13 % Al2O3, Si = 5.7) (W.R. Grace & Co., USA), and hydrogen (Airgas, Inc., USA) were used in the conversion processes. Analysis of hydrotreatment products was conducted using an Agilent 5975C GC/MSD system (HP-5, Column), two-dimensional gas chromatography (GC × GC) with flame ionization detector (FID), CHN analyzer (CHN 628, LECO Corporation, USA), a 600 MHz Bruker Avance III NMR Spectrometer (Bruker Corporation, USA), and an Agilent HPLC 1100 system (Agilent Technologies, Inc., USA) with a Waters C18 reversed-phase column (Waters Corporation, USA).

2.9. Fuel property analysis

NREL Fuels and Combustion Science group used ASTM standards, including D2887, D5972, and D6450 [34–36] to determine the fuel properties of the hydrocarbon product derived from paper sludge. The Bioproducts, Sciences, and Engineering Laboratory at Washington State University (BSEL-WSU) applied prescreening methods, tier α (predictive aspects) for composition and distillation analysis, and tier β to directly measure fuel-critical properties of the hydrocarbon product, as described by Heyne *et al.* [37].

2.10. Alternative process configurations

In the techno-economic analysis (TEA), nine biorefinery configurations are compared. The base case follows the catalytic pathway outlined by Klein *et al.* [20], using petroleum-based (PB) MEK, a 20 % fiber consistency for enzymatic hydrolysis, a 20 % sugar mass fraction for dehydration, and a 1.75:1 vol ratio of 1,4-dioxane to aqueous sugar solution for the dehydration step. Five key process modifications are analyzed: MEK source (petroleum-based vs. biobased), fiber consistency, sugar mass fraction, organic solvent-to-aqueous volume ratio, and the replacement of 1,4-dioxane with acetone as the organic solvent in the dehydration reaction step. Detailed process modifications are presented in Table 1.

2.11. Process design and modeling

The reliability of a techno-economic and sensitivity analysis depends on the accurate determination of the mass and energy balance across the evaluated biorefinery, which is essential for estimating operational and capital expenditures. Aspen Plus™ (v11) was utilized in this study to model the mass and heat balances across the various process units. The "Corn stover to ethanol" model developed by NREL, available in the Aspen Plus™ (v11), including components specifications and property sets, served as the baseline for the simulation files used in this work. A Microsoft Excel® file was created to estimate the facility's power demand based on the specific equipment power consumption, as detailed in supporting information (*Supplementary material, S17*). This same file integrated mass, heat, and power flows with labor, materials, and equipment costs, as well as financial parameters and correction indices, to perform a discounted cash flow rate of return (DCFROR) analysis. Additionally, macros were employed to vary process and financial/economic variables for sensitivity analysis in each case study. Due to limitations in linking the sensitivity analysis file with Aspen Plus™ (v11) to determine the heat balance across the facility following material flow changes caused by variations in process variables as part of the sensitivity analysis, the heat and cooling demand results for the baseline case in each study, as estimated in the simulation files, were scaled based on the updated mass flow entering each piece of equipment, as recalculated in the sensitivity analysis file. Given that the process design depends on experimental results and operational conditions, and to ensure logical temporal consistency, the detailed modeling assumptions are discussed in Section 3.9 of this document.

2.12. sEconomic evaluation

A discounted cash flow rate of return (DCFROR) analysis was conducted to determine the minimum fuel selling price of the hydrocarbon product derived from paper sludge and to evaluate the biorefinery's investment potential. The financial parameters and correction indices used, based on NREL reports [20,38,39], are presented in Table 2.

2.12.1. Fixed capital investment

The Fixed Capital Investment (FCI) is estimated by adding the total depreciable capital, which includes the Total Direct Cost (TDC) and Total Indirect Cost (TIC). TDC includes the Total Installed Equipment

Table 1
Major process conditions and modifications for the base case and alternative case studies. Biorefineries using (a) 1,4-dioxane (base case and alternative cases 1 through 4) or (b) acetone (alternative cases 5 through 8) as organic solvent during the sugar dehydration reaction.

Process variable	Base case	Alternative cases 1 & 5	Alternative cases 2 & 6	Alternative case 3 & 7	Alternative case 4 & 8
Methyl ethyl ketone source	**Petroleum-based (PB)**	**Biobased**	Biobased	Biobased	Biobased
Fiber consistency for enzymatic hydrolysis	20 %	20 %	20 %	**30 %**	20 %
Sugar mass fraction in solution for the dehydration reaction	20 %	20 %	20 %	30 %	**40 %**
Organic solvent-to-aqueous sugar solution volume ratio for the sugar dehydration reaction	1.75	1.75	**1.50**	1.75	1.75
Evaporator before dehydration reactor to increase sugar mass content	No	No	No	No	**Yes**

Table 2
Financial parameters and cost indices used in the techno-economic analysis (DCFROR) and the sensitivity assessment, based on NREL Technical Reports [20,38,39].

Item	Value
Equity financed	40 %
Loan term	10 years
Loan interest	8 %
Working capital (% of FCI)	5 %
Depreciation period – General plant	7 years (MACRS) [71]
Depreciation period – Heat & power / Utilities	20 years (MACRS) [71]
Construction period	3 years
Project lifetime	30 years
Start-up time	3 months
Discount rate: Internal rate of return	10 %
Income tax rate	21 %
Annual operating time	7,884 h
Cost year for analysis	2024
Chemical Engineering Plant Cost Index (CEPCI)	795.1 (January 2024) [40]
Producer Price Index: Chemical Manufacturing (PCU325325)	356.5 (August 2024) [72]
Labor Index: Chemical Manufacturing (CEU3232500008)	30.6 (August 2024) [73]

Cost (TIEC) for areas A100 to A700, along with the cost for the warehouse (4 % of the inside battery limits, ISBL: A100 to A500), site development (10 % ISBL), and additional piping (4.5 % ISBL). TIC, estimated based on TDC, includes prorateable expenses (10 % TDC), field expenses (10 % TDC), home office & construction fee (20 % TDC), project contingency (10 % TDC), and other costs (e.g., start-up, permits, etc.,) (10 % TDC). The Total Capital Investment (TCI) is calculated by adding the FCI, land cost ($1.85 MM), and working capital (5 % FCI), following NREL reports [38]. Additional definitions are provided in the supporting information (*Supplementary material, S19*).

2.12.2. Equipment cost

The size of the 120 pieces of equipment used in each biorefinery was determined based on the process mass balance, supported by the results of the Aspen Plus™ (v11) simulation model. The equipment cost for areas A100 to A700 was scaled using reference purchase equipment costs, scaling exponents from NREL reports [20] and the power law equation, **Eq. (1)**. To reflect 2024 prices, cost adjustments were made using the Chemical Engineering Plant Cost Index (CEPCI) [40], as outlined in **Eq. (2)**. The equipment inventory used in the techno-economic analysis of the base case scenario is provided in the supporting information (*Supplementary material, S17*).

$$NewEquipmentCost = ReferenceCost\left(\frac{NewScalingValue}{ReferenceScalingValue}\right)^{ScalingExponent} \quad (1)$$

$$Cost_{2024} = Cost_{referenceyear} \times \frac{CEPCI_{2024}}{CEPCI_{referenceyear}} \quad (2)$$

2.12.3. Annual total operating cost

The Total Operating Cost (TOC) is calculated by adding the Variable Operating Cost (VOC) and Fixed Operating Cost (FOC). The VOC is assessed using stream flow rates and mass and energy balances from the Aspen Plus™ (v11) process simulations. Table 3 details the prices of chemicals and utilities along with the value of production credits. The FOC is calculated by adding the Total Labor Salaries (TLS), which are estimated based on plant personnel salaries (Bureau of Labor Statistics, Series ID: CEU3232500008) [31], along with overhead (90 % TLS), maintenance (3 % ISBL), and property insurance (1 % FCI).

2.12.4. DCFROR model and sensitivity assessment

The Discounted Cash Flow Rate of Return (DCFROF) method was employed to calculate the MFSP at which the Net Present Value (NPV) of the biorefinery over its project lifetime, *N*, as described in **Eq. (3)**, equals zero.

$$NPV = \sum_{t=1}^{N}\left[\frac{CF_t}{(1+i)^t}\right] \quad (3)$$

A sensitivity assessment was conducted to evaluate the impact of seventy-five process, economic, and financial uncertainties on the MFSP of the resulting hydrocarbon product derived from paper sludge across each of the nine biorefinery configurations analyzed. Table 4 presents the most relevant process variable specifications, derived from experimental results and used as the baseline for the sensitivity assessments.

Table 3
Cost of materials and value of credits in reference year used to estimate the Total Operating Cost in 2024 U.S. dollars.

Material	Price (reference year)	Reference
Process makeup water	$0.44/mt (2016)	[38]
Enzyme	$6,160/mt (2016)	[38]
Hydrochloric acid (HCl)	$108/mt (2011)	[39]
1,4-Dioxane	$1,684/mt (2016)	[20]
Acetone	$992/mt (2018)	[74]
Aluminum chloride	$800/mt (2019)	[75]
Methyl ethyl ketone (Petroleum Based)	$1,650/mt (2019)	[74]
Methyl ethyl ketone (Biobased)	$660/mt (2016)	[20]
Sodium hydroxide (NaOH)	$526/mt (2016)	[38]
Hydrogen	$1,611/mt (2016)	[38]
HDO Catalyst (Pd/C)	$651/lb (2016)	[38]
Boiler chemicals	$6,564/mt (2016)	[38]
Cooling tower chemicals	$3,933/mt (2016)	[38]
Natural gas	$2.53/MMBTU (2023)	[76]
Credit	**Credit value**	**Reference**
Paper sludge disposal credit	$60/mt (dry) (2019)	[77,78]
Power (retail price / industrial)	¢8.06/kWh (2023)	[79]

Table 4
Summary of operation conditions and process variables used as the baseline in the techno-economic analysis and the sensitivity assessment.

Area	Process	Specifications	Reference
A100	Feedstock handling	Biorefinery size: 750mt of paper sludge per day (OD)	Paper mills producing more than 100 CE mt/day of paper sludge [58].
A200	Pretreatment	Ash removal: 95 %	Lab scale and pilot plant scale experimental results [41]
		Carbohydrates retention: 95 %	Lab scale and pilot plant scale experimental results [32]
A300	Enzymatic hydrolysis	**Enzymatic hydrolysis**	
		Reaction temperature: 50 °C (optimal)	Experimental results
		Enzyme loading: 10 mg protein/g cellulose	Experimental results
		Carbohydrates conversion: 99 %	Experimental results
		Yield of sugars: 99 %	Experimental results
A400	Catalytic conversion and upgrading	**Sugar dehydration reaction**	
		Reaction temperature: 190 °C (optimal)	Experimental results
		Catalyst loading: 10 mM $AlCl_3$	Experimental results
		Glucose conversion: 97 %	Experimental results
		Xylose conversion: 95 %	
		1,4-dioxane systems (Operating pressure: 1,660 kPa)	Experimental results
		Yield of 5-HMF: 71 %	
		Yield of furfural: 84 %	
		Acetone systems (Operating pressure: 2,350 kPa)	Experimental results
		Yield of 5-HMF: 68 %	
		Yield of furfural: 82 %	
		Solvent loss: 1 %	[80]
		Aldol-condensation reaction	
		Reaction temperature: 50 °C	Experimental results
		1,4-dioxane systems	Experimental results
		NaOH loading: 0.91 (mole of Furan to mole of NaOH)	
		Acetone systems	Experimental results
		NaOH loading: 0.55 (mole of Furan to mole of NaOH)	
		5-HMF conversion: 99.6 %	[49]
		Furfural conversion: 99.6 %	[49]
		Yield of monoadducts: 95.5 %	[49]
		Yield of diadducts: 4.1 %	[49]
		Hydrogenation reaction	
		Reaction temperature: 100 °C	
		Hydrogen loss: 5 %	Assumed
		Monoadducts and diadducts conversion: 96.3 %	[49]
		Yield of hydrogenation products: 73 %	[49]
		Hydrodeoxygenation reaction	
		Reaction temperature: 300 °C	Experimental results
		Hydrogen loss: 5 %	Assumed
		Catalyst weight hourly space velocity: 2 $h^{(-1)}$	[38]
		Catalyst lifetime: 2 years	[38]
		Hydrogenation products conversion: 96.3 %	[49]
		Yield of hydrocarbons: 73 %	[49]
A500	Wastewater treatment	Process water recycled: 80 %	Assumed
A600	Heat and power	Boiler condensate recycled: 80 %	Assumed
A700	Utilities	Cooling water temperature 25 °C	Assumed

3. Results and discussion

3.1. Paper sludge characterization

Paper sludge composition varies depending on paper mill operation conditions. Based on the analysis of samples collected from the Kraft pulp mill producing uncoated freesheet, the paper sludge used in this study had a mean consistency of 50 % total solids, with 43.7 % ash, 30.5 % glucan, 8.5 % xylan, 3.3 % arabinan and mannan, and 3.1 % lignin. Calcium compounds were the major contributors to the inorganic fraction. Detailed characterization results are available in previously published materials [32].

3.2. Ash removal

As detailed in a previous investigation by this research group, the optimal results obtained in the bench-scale Pulmac Master™ device were achieved with a 0.2 mm slot opening screen plate, resulting in 99 % ash removal and 63 % carbohydrate retention [32]. Paper sludge with an initial total solids content of 33 %-50 % was mixed with municipal water in the hydro pulper to explore optimal process conditions at the pilot scale. The static Sidehill screen system with a 0.25 mm slot opening outperformed lab-scale experiments in carbohydrate retention. At the optimal 3 % total solids content (31 kg of municipal water per kg of oven-dry paper sludge processed), the pilot-scale equipment achieved over 95 % ash removal and 95 % carbohydrate retention. Further details on these remarkable results are available in a previous publication [41]. A total of 30 OD kg of deashed paper sludge was obtained from the pilot-scale system and sent to NREL for large-scale hydrolysis.

3.3. Enzymatic hydrolysis

The optimal enzymatic hydrolysis conditions were determined at a bench scale, as detailed in a previous work [32]. Based on these findings, the pilot plant scale 30-L paddle-type batch reactor system operated at 65 rpm, 50 °C, with 15 wt% solids, an enzyme loading of 15.65 mg protein/g cellulose, and an initial pH of 5.0, adjusted using a 1 M hydrochloric acid (HCl) solution. Hydrolysis ran for 96 h, producing 35 L of sugar hydrolysate over three batches. These experiments achieved a maximum cellulose conversion of 78.7 %, and a xylan conversion of 100 %, yielding 3.9 kg of combined sugars (87.6 g/l of glucose and 23.2 g/l of xylose). The pilot plant scale carbohydrate conversion approached the bench scale results (99.5 % max.) and exceeded results in the literature (60 %) [42].

3.4. Sugar dehydration

Adding an organic solvent during glucose and xylose dehydration in aqueous solutions can enhance 5-HMF and furfural yields [43]. The catalyst-solvent system plays a significant role in maximizing product yield while minimizing side reactions [44]. NREL achieved optimal results using aluminum chloride, a Lewis acid catalyst, and 1,4-dioxane to dehydrate sugars derived from lignocellulosic biomass [20]. However, the azeotrope in the 1,4-dioxane/water system at 82 wt% solvent and 87.6 °C under atmospheric conditions [45] represents a thermodynamic barrier for solvent purification and leads to excess water recycling when conventional distillation is employed to recover and reuse this cyclic ether. In the search for strategies to potentially overcome this

thermodynamic limitation, eight alternative solvents (acetone, THF, MEK, 2-butanol, ethyl acetate, DMSO, MIBK, methanol) were evaluated against 1,4-dioxane based on their physicochemical properties and previous solvent screenings [44]. Among the evaluated solvents, acetone provided a 5-HMF yield closest to 1,4-dioxane (*Supplementary material, S1*). Therefore, this volatile ketone was selected for further analysis as a potential alternative to 1,4-dioxane.

Based on preliminary simulation results regarding the heat demand for the solvent recovery step, acetone, being the less heat-demanding system (in contrast to 1,4-dioxane) due to its lower boiling point and the absence of an azeotrope with water, was selected for scaling up the production of 5-HMF and furfural from paper sludge hydrolysate using a continuous flow reactor at NREL. Process variables, such as reaction temperature, catalyst loading, and residence time, were optimized to maximize the product yield. A maximum yield of 68 % for 5-HMF and 82 % for furfural (with 98 % glucose conversion and 96 % xylose conversion) were achieved at 190 °C, 7.5 mM $AlCl_3$, 9-minute residence time, at a 2:1 acetone to aqueous volume ratio. The continuous flow reactor was used to produce 50 L of furans solution (10 g/l 5-HMF and 2.5 g/l furfural) at a rate of 1.5 L/day, resulting in 0.63 kg of combined furans. In comparison, identical reaction conditions with 1,4-dioxane resulted in a 71 % 5-HMF yield and an 84 % furfural yield. The optimized yields of 5-HMF and furfural achieved were substantially higher than those reported in the literature. For example, Xin *et al.* [46] reported a 48 % 5-HMF yield using aluminum chloride and 1,4-dioxane, while Zhu *et al.* [47] reported a 64.5 % 5-HMF yield with $AlCl_3$ and acetone at a 4:1 organic-to-aqueous volume ratio, double that used in this study. During the production of furans from paper sludge hydrolysate in the continuous flow reactor, dark deposits of side products, such as humins, accumulated on the inner surface of the reactor's heating zone, requiring removal to maintain efficiency and avoid potential process disruptions. This observation is crucial for industrial applications, as reactor fouling can significantly impact long-term operational stability.

3.5. Aldol-condensation and solvent recovery

Aldol-condensation follows the production of 5-HMF and furfural (Fig. 1) to increase carbon atoms in the resulting intermediate oxygenated adducts, targeting C_9 and C_{10} so that the final hydrocarbon blend falls within the C_8-C_{16} jet fuel range [48]. Since 5-HMF and furfural contain six and five carbon atoms, respectively, methyl ethyl ketone (MEK) is used as a reactant in this step. Sodium hydroxide (NaOH) acts as a catalyst, initiating the reaction by abstracting an α-hydrogen from the primary or secondary carbon adjacent to the carbonyl group in MEK [49]. Depending on the location of the α-hydrogen abstracted, the relative abundance of the reactants, and other reaction conditions, different monoadducts, and diadducts, can be formed (Fig. 1). In systems using 1,4-dioxane during the sugar dehydration step (Fig. 2**a**), the presence of this solvent is not expected to significantly impact the aldol-condensation reaction. However, in systems using acetone, 5-HMF and furfural could partially condense with this organic solvent [50], yielding C_7 and C_8 condensation products. Therefore, if acetone is used as an organic solvent during sugar dehydration step, it must be completely removed before the aldol-condensation reaction. This explains the need to relocate the solvent recovery system, as depicted in Fig. 2**b**. Initial aldol-condensation experiments at NREL were performed in the presence of 1,4-dioxane at a catalyst load of 1.1 mol of NaOH per mole of combined furans (pH ~ 13.8) and 2.5 mol of MEK per mole of combined furans (favoring monoadducts formation) at 80 °C for 40 min. However, additional experiments became necessary due to the shift in solvent handling strategy when acetone was used in large-scale continuous dehydration experiments.

The 5-HMF and furfural solution containing organic solvent produced in the continuous dehydration reactor at NREL was processed at NCSU at 10.5 ml/min using the in-house-built distillation system to remove acetone. HPLC results confirmed the absence of acetone in the bottom product and the high purity of the distilled stream (99.8 % acetone). A dark solid material was deposited on the lower separation stages near the reboiler during the distillation, as observed in the continuous dehydration experiment. A water bath reactor was used to optimize both temperature and time for the aldol-condensation reaction to maximize monoadduct product content. A catalyst load of 1.8 mol of NaOH per mole of combined furans (pH ~ 13.0) and 2.0 mol of MEK per mole of combined furans were used. In contrast to aldol-condensation experiments involving 1,4-dioxane, a highest NaOH loading was necessary to raise the pH to appropriate levels, as the removal of the organic solvent increased the concentration of acidic species generated by side reactions during the dehydration of sugars (e.g., levulinic acid, formic acid, etc.,) [33]. Reaction temperature ranging from 24 °C to 80 °C and reaction time between 10 and 80 min were evaluated, with 50 °C and 10 min identified as the optimal conditions, contrasting with other studies using higher reaction temperature (>120 °C) and longer reaction time (>4 h) [51,52]. The reaction was scaled up in a 5-L stirred batch reactor. A total of 0.22 kg of aldol-condensation product was obtained and sent to NREL for hydrotreatment.

3.6. Low-temperature hydrogenation

The isolated aldol-condensation product was hydrogenated under mild conditions to stabilize it before being subjected to more severe conditions necessary for HDO [53]. The hydrogenation was carried out in 75-ml stirred Parr batch reactors at 100 °C for 2 h, at 68 bar of H_2, and palladium catalyst with acidic support (7.4 g product per g catalyst Pd/SiO_2-Al_2O_3). This process aimed to hydrogenate the C–C double bonds present in the furfural rings and the side chain of the adducts (Fig. 1). During the reaction, 0.28 g of H_2 were consumed per gram of adduct. The isolated yield of the hydrogenated adduct (H-adduct) from three batches was 95.7 wt%, which is considerably better than previously reported yields ranging from 70 % to 80 % [54]. ^{13}C NMR results show the effectiveness of hydrogenation with the disappearance of almost all peaks in the 100 to 160 ppm region, and a corresponding increase in peaks in the 0 to 90 ppm region, indicating conversion of unsaturated carbons. However, the carbonyl groups in the adducts remained unaffected, as indicated by the retention of the peaks in the 200 to 220 ppm region (Fig. 3**a** & Fig. 3**b**). LC-MS (*Supplementary material, S2*) and GC/MS (Fig. 3**d**) confirmed the successful hydrogenation of C–C double bonds, and elemental analysis (CH) showed that the H/C ratio of the H-adduct increased from 1.26 to 1.73 (*Supplementary material, S13*).

3.7. Hydrodeoxygenation reaction

HDO was performed on the H-adducts in stirred Parr batch reactors at 300 °C for 3 h under 68 bar of H_2, using either a Pd or Pt catalyst supported on a SiO_2-Al_2O_3. Methylcyclohexane was employed as a diluent for H-adducts, to promote the H_2 solubility and faster reaction kinetics [55]. HDO experiments were conducted to examine the effect of different metal catalysts and the H-adducts loading on reaction outcomes. The low-temperature hydrogenation products were successfully converted into the expected hydrocarbons: n-decane, 3-methyl nonane, n-nonane, and 3-methyl octane (C_9-C_{10}), derived from the H-monoadducts, as well as small amounts of hydrocarbons such as 6-methyl tridecane and 7-methyl pentadecane (C_{14}-C_{16}), originating from the H-diadducts (Fig. 3**c** & Fig. 3**d**). In addition, small amounts of cycloalkanes were identified in the hydrocarbon product by GC/MS, including ethyl cyclohexane, butyl cyclohexane, and methyl propyl cyclohexane, suggesting some cyclization ability of the acid catalyst. The Pt and Pd catalysts appeared equally effective. However, an H-adduct loading of 2.16H-adduct/catalyst weight ratio or lower is required for the complete hydrogenation of H-adducts. Higher H-adduct loadings (2.17 to 7.8) resulted in the formation of oxygenated products, such as 3-decanoate and 3-nonanone, along with some cyclohexanones, as observed

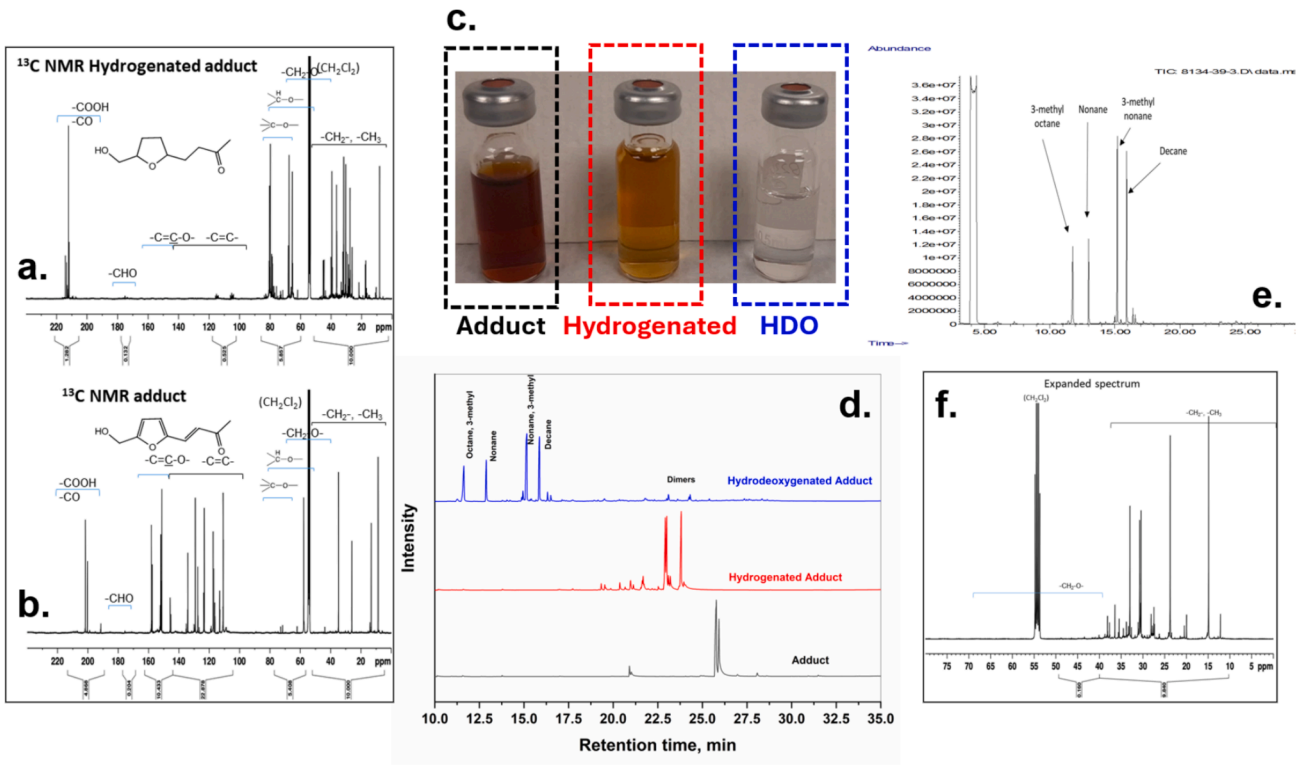

Fig. 3. ^{13}C NMR of adduct mixture after (a) and before (b) hydrogenation. (c) Aldol adducts, hydrogenated adducts, and HDO hydrocarbon products. (d) GC/MS of aldol adducts before and after low-temperature hydrogenation and HDO products. (e) GC/MS of final hydrocarbon product, and (f) ^{13}C NMR spectrum of final hydrocarbon product from paper sludge.

in the GC/MS analysis (*Supplementary material, S14 & S15*). A second set of five HDO experiments was performed at the lowest loading level (2.16 to 2.18) to test the reproducibility of the HDO reaction using Pt on the SiO_2-Al_2O_3 support. All HDO reactions were reproduced in product distribution with an average isolated yield of 54 ± 0.7 wt%, below the typical yield reported in the literature (65 % – 87 %) [55,56], indicating the need for additional optimization of this transformation step. All five resulting samples were combined and subjected to a second HDO to further convert the remaining oxygenated products. A total of 40 g of hydrocarbon blend, equivalent to 50 ml, was obtained and split into two aliquots for analysis at two independent laboratories for fuel property testing.

3.8. Fuel properties analysis

The GC–MS (Fig. 3**e**) and GC × GC analyses reveal that the final hydrocarbon product (HC) contains the expected n-alkanes and *iso*-alkanes in the C_9-C_{10} range, produced by hydrodeoxygenation of mono-adducts from 5-HMF and furfural with MEK. HDO of diadducts also formed small amounts of C_{14}-C_{16} *iso*-alkanes. Unexpectedly, a small quantity of cycloalkanes, which have favorable fuel properties due to their higher energy density, is also observed. Both iso- and n-alkanes are present in similar amounts, suggesting that aldol condensation occurred at similar rates at the methyl and methylene carbons in MEK. The ^{13}C NMR spectrum of the final hydrocarbon product (Fig. 3**f**) shows no peaks in the carbonyl/ketone (−C(=O)-), carbonyl/aldehyde (–CHO), or carboxylic acid (–COOH) regions. This indicates that the HDO product is almost entirely composed of hydrocarbons, with little to no oxygenated carbons, as nearly all the signal intensity appeared in the 10 to 40 ppm range.

Results from the NREL Fuels and Combustion Science group show that the HC product has low oxygen content (0.2 wt%), a freezing point of −57.1 °C (within jet fuel specifications), and a flash point of 46.7 °C, meeting Jet A standards [57], with the energy density exceeding jet fuel requirements (46.8 MJ/kg) (*Supplementary material, S16*).

As determined in the tier α analysis by BSEL-WSU, the HDO product contains a mix of n-alkanes (34 %), *iso*-alkanes (43 %), and cycloalkanes (22 %), making it more versatile for blending into jet and diesel fuels compared to other biofuels dominated by a single hydrocarbon type (*Supplementary material, S3*). The simulated distillation analysis, performed by BSEL-WSU according to ASTM D2887 [34] and compared to conventional aviation fuel [37], shows that about 44.3 % of the hydrocarbons produced from paper sludge fall within the jet fuel boiling range (156 °C – 293 °C), making them suitable for blending into jet fuel. The results indicate that more than 50 % of the final hydrocarbon product could be blended into jet or diesel fuel. The distilled cut within the jet fuel boiling range was analyzed for predictive components of critical properties (tier β) by BSEL-WSU via ASTM test methods and the prescreening test described by Heyne *et al.* [37]. All fuel-critical properties except density were within ASTM specifications limits, with the heat of combustion exceeding Jet A requirements (Table 5). Overall, test results for critical jet fuel properties, as determined by two independent laboratories, were consistent for most properties tested, supporting the strong potential of the hydrocarbon product derived from paper sludge as a Jet A drop-in fuel.

3.9. Simulation: General assumptions based on experimental results

To avoid data duplication, some process conditions used in the simulated biorefinery studies (based on experimental results) are not mentioned in this section, as their details are provided in Sections 3.1 to 3.8. Key reaction parameters are also summarized in Table 4.

The baseline biorefinery processing capacity is set at 750 CE mt/day of paper sludge, based on data from thirteen paper mills in the southeastern U.S. that generate over 100 CE mt/day of paper sludge (*Supplementary material, S4*) [58]. In the **A100** feedstock handling area, paper sludge is weighed on a truck scale and transferred using a truck dumper and a series of transfer conveyors for storage in a dome reclaim

Table 5
Fuel-critical physicochemical properties determined for the distilled cut of hydrocarbon product derived from carbohydrates in paper sludge, conducted at BSEL-WSU.

Parameter	Hydrocarbon product	Units	ASTM specification limits**
Surface tension, σ (22 °C)	24.2	mN/m	Not specified
Density, ρ (15 °C)	753	kg/m^3	775 to 840
Viscosity, ν (−20 °C)	2.8	cSt	8 max.
Viscosity, ν (−40 °C)	4.9	cSt	12 max.
Net Heat of Combustion (LHV)	44.0	MJ/kg	42.8 min.
Flash point	47.5	°C	38 min.
Derived Cetane Number (DCN)	48.3	DCN	Not specified
Freeze point	−42.9	°C	−40 max.

* ASTM D7566 Standard specifications for aviation turbine fuel containing synthesized hydrocarbons [11].

system. In the **A200** pretreatment area, paper sludge is transferred to a pulper tank and mixed with recycled process water to achieve a 3 % total solids content. It is then pumped to a fiber retention system for ash removal, achieving 95 % ash removal and 95 % carbohydrate retention. Considering the variability in the solids content of paper sludge and the challenges in achieving a perfect mass balance closure in experimental compositional analysis, the total solids content of this material is set at 50 %, and the distribution of solid materials based on experimental results is proportionally expanded to cover 100 %. On a dry basis, the composition used in the simulation comprises 49 % ash, 47 % total carbohydrates (33.9 % glucan, 9.3 % xylan, and 3.8 % mannan), and 4 % lignin. In **Area 200**, deashed wet fibers with 20 % total solids content are transported via transfer screw systems to the acidification tank to achieve the optimal pH for enzymatic hydrolysis treatment (initial pH 3.1), using hydrochloric acid (7.3 mg of HCl per gram of deashed paper sludge). In the **A300** enzymatic hydrolysis area, the pretreated fiber suspension is pumped to an in-line mixer, where the fibers are combined with cellulase (10 mg of enzyme per gram of cellulose, equivalent to approximately 5 Filter Paper Units per gram of deashed sludge – Cellic® Ctec2, Novozymes) before entering the enzymatic hydrolysis reactor with an agitation system. In the reactor, the fibers are treated at 50 °C for 96 h. After the reaction, the product is transferred to a solids removal system, and the filtered hydrolysate is pumped into a storage tank. A carbohydrate conversion of 99 % and a yield of 99 % to glucose and xylose are assumed in the simulation. The **A400** catalytic conversion and upgrading area comprises four catalytic reaction steps and a solvent recovery system. Following enzymatic hydrolysis, the filtered hydrolysate is pumped to an in-line mixer where it is combined with 1,4-dioxane or acetone (at a 1.75:1 organic solvent to aqueous sugar solution volume ratio) and aluminum chloride (10 mM $AlCl_3$) before entering the dehydration reactor, which operates at 190 °C. Reaction parameters, including sugar conversion, reactor operating pressure, and furans yields for each solvent system analyzed, are presented in Table 4. After producing 5-HMF and furfural, a distillation column system is used to recover the organic solvent used in the dehydration reactor. The complexity of the heat and mass transfer phenomena occurring inside this equipment, along with the azeotropic interactions between water and 1,4-dioxane, requires validating the thermodynamic method used to simulate this separation stage. Following a comparison of experimental data [45,59–61] and confirmation of the simulation results' accuracy, the NRTL-2 thermodynamic method was selected and used in the Aspen Plus™ (v11) simulation files. According to simulation results, 10 total theoretical equilibrium stages and a feed stage at the fourth plate (5th stage) are sufficient to recover 99 % of the organic solvent at 80 wt% concentration for 1,4-dioxane (near the azeotropic concentration) and 98 wt% purity for acetone systems. As previously discussed, the organic solvent recovery step is positioned after the low-temperature hydrogenation reactor in scenarios using 1,4-dioxane and after the dehydration reactor in scenarios using acetone. **A400** also includes the aldol-condensation reactor, operating at 50 °C, and storage and transfer systems for methyl ethyl ketone, sodium hydroxide, and hydrophobic aldol-condensation products. The techno-economic analysis presented here does not account for aldol-condensation catalyst recovery; fresh sodium hydroxide is used in each case study. Additional reaction assumptions are provided in Table 4. This area also includes two hydrogenation facilities equipped with hydrogen recovery systems for the low-temperature hydrogenation of the decanted aldol-condensation products and the subsequent hydrodeoxygenation reaction. Following NREL assumptions, the baseline considers a 5 % hydrogen loss and a solid catalyst weight hourly space velocity of 2.0 hr^{-1}, with a catalyst lifetime of 2 years [20]. The **A500** wastewater treatment area consists of an aeration basin with nine blowers, a membrane bioreactor, a centrifuge system, transfer conveyors, transfer pumps, and supporting equipment for wastewater treatment chemicals such as ammonia and others (*Supplementary material, S17*). The **A600** heat and power area includes a natural gas boiler to produce superheated steam at a manometric pressure of 4,137 kPa and 300 °C (80 % boiler efficiency and 5 % boiler blowdown) to supply the hydrodeoxygenation reactor and a steam turbine generator (85 % turbine efficiency) with a steam outlet pressure of 1,034 kPa and 216 °C, used for plant heating services (assuming a 5 % loss in pipelines to the surroundings). The required steam production from the boiler is calculated considering the facility's heat demand (*Supplementary material, S18*) after crossing hot and cold streams using heat exchangers listed in the equipment inventory (*Supplementary material, S17*). Power generation is determined based on the steam required for heating. A power surplus can occur if the facility's heat demand causes the generated power to exceed the plant's power requirement. **A600** also includes equipment such as a deaerator, a hot process water softener system, boiler water treatment chemicals addition systems (amine, ammonia, phosphate, etc.), transfer pumps, and a condensate collection tank, among others. The **A700** utilities area includes cooling towers, air compressor systems, a chilled water package, a process water tank, and a main cooling water pump. The required amounts of cooling water and cooling tower chemicals are estimated based on additional cooling service requirements (*Supplementary material, S18*) and the specific enthalpy of sub-cooled water at 25 °C and 101.325 kPa. A process water recovery rate of 80 % and boiler condensate recycling rate of 80 % are assumed in the simulation. Detailed results on mass balance, raw materials, and heat and power flows are provided in the supporting information (*Supplementary material, S5-S12, and S18*).

3.10. Energy return on investment

Evaluating the efficiency of bio-based energy production systems is crucial in biorefinery analysis. The Energy Return on Investment (EROI), or "net energy," measures the ratio of usable energy produced to the energy required for production [62]. An EROI above 1 indicates a positive energy balance. Biorefineries using 1,4-dioxane for sugar dehydration show an EROI < 1, indicating energy input exceeds output. In all four biorefineries using acetone, the EROI exceeds 1.81, peaking at 3.25 for alternative case 7 (EROI: 3.25). These values align with other biorefinery analyses, such as corn-to-ethanol (EROI: 0.82–1.73) [63], microalgal biomass-to-biodiesel (EROI: 0.87) [64], and soybean-to-biodiesel (EROI: 3.10) [65]. The computed EROI values and process yields (GGE per kg of carbohydrates and GGE per kg of combined carbohydrates and methyl ethyl ketone) for each analyzed case are detailed in supporting information (*Supplementary material, S18*).

3.11. Biorefinery production capacity

Continuous flow reactor experiments at NREL showed that the highest yields of 5-HMF and furfural were achieved using 1,4-dioxane

compared to acetone (Table 4). This difference explains the variations in hydrocarbon blend production capacities between systems utilizing 1,4-dioxane (24.88 MM GGE/year) and those using acetone (23.86 MM GGE/year).

3.12. Minimum fuel selling price

The MFSP of the hydrocarbon product from paper sludge for the nine biorefinery configurations is summarized in Fig. 4. The base case resulted in an MFSP of $8.6/GGE, with a Total Capital Investment of $434MM, primarily driven by the installed cost of A400 ($87.7MM) and A600 ($79.6MM) as Other Direct + Indirect Capital Costs ($202MM) are dependent on the Total Installed Equipment Cost. The Total Operating Cost for the same base case is estimated at $160MM/year, primarily influenced by the cost of petroleum-based MEK ($72.4MM/year). However, when the source of MEK is switched from the base case to alternative case 1, using the transfer price of biobased MEK produced via sugars fermentation to 2-butanediol (BDO) with an engineered strain of *Zymomonas mobilis*, followed by catalytic upgrading of BDO, as outlined in [20], the MFSP decreases to $6.9/GGE.

Reducing the organic solvent-to-aqueous sugar solution volume ratio from 1.75:1 (alternative case 1) to 1.5:1 (alternative case 2) lowers the Variable Operating Cost (VOC) (Fig. 5**b**) and MFSP to $6.3/GGE, mainly due to reduced 1,4-dioxane loss (fixed at 1 % solvent entering the distillation system). Increasing fiber consistency for enzymatic hydrolysis to 30 % in alternative case 3 further reduces the MFSP to $5.6/GGE by reducing the volume of 1,4-dioxane needed to maintain a 1.75:1 solvent-to-aqueous volume ratio and the reduction in solvent loss. Similarly, in alternative case 4, the same effects are observed after adding an evaporation unit to increase the sugar content to 40 % before the dehydration step, further lowering the MFSP to $5.2/GGE (Fig. 2**b**). In alternative cases 5 to 8, replacing 1,4-dioxane with acetone lowers the MFSP despite reduced hydrocarbon yield. The key factors explaining this include acetone's lower price (reduced TOC) (Fig. 5**b**), decreased solvent loss, and a smaller TCI due to a reduced A600 (Heat and power area) (Fig. 5**a**). The combined effects of acetone's higher volatility

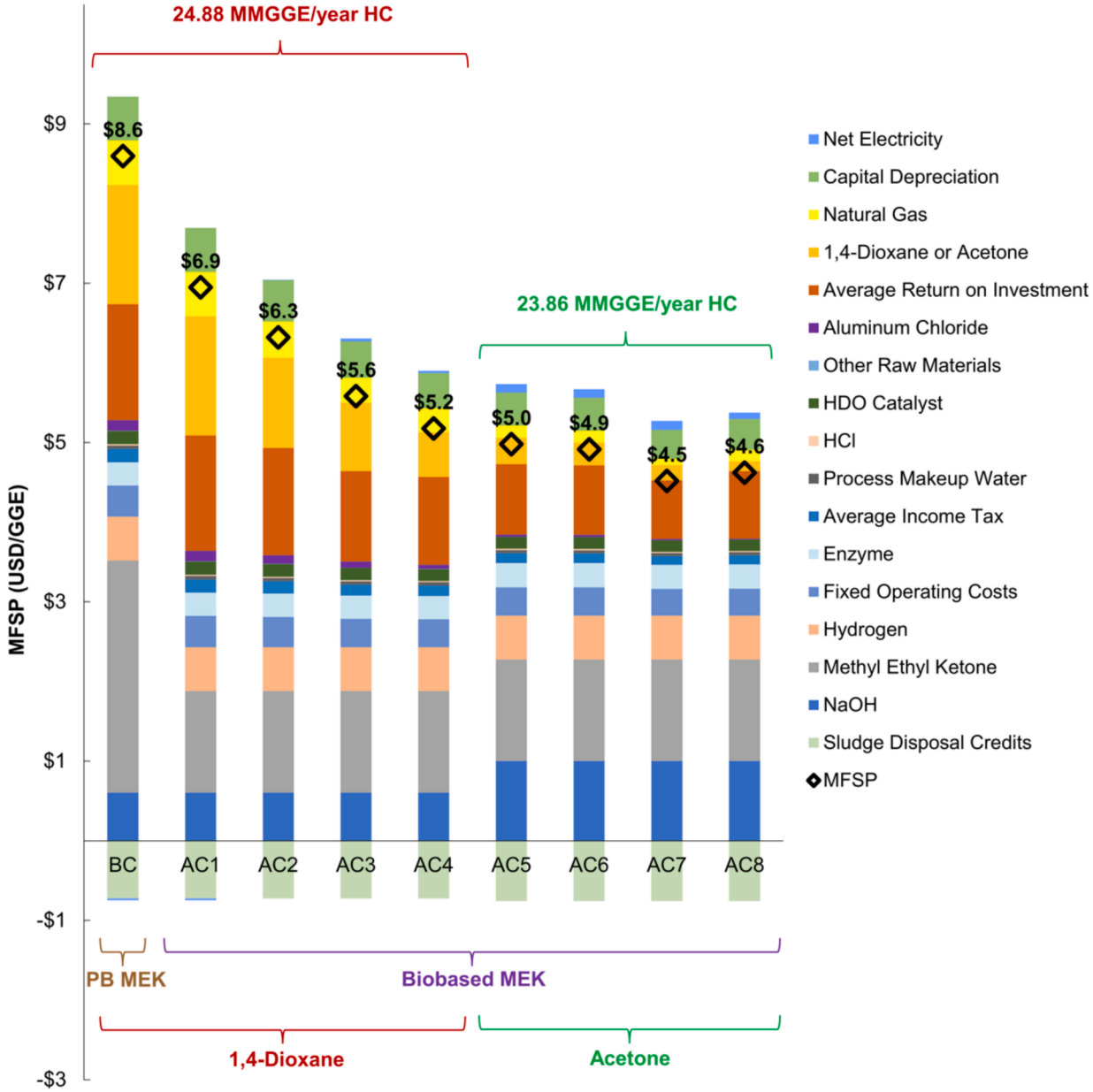

Fig. 4. Minimum Fuel Selling Price of the hydrocarbon product derived from carbohydrates in paper sludge (diamonds) for the base case and alternative cases 1 through 8 and share distribution of manufacturing costs (stacked columns) (2024 U.S. dollars).

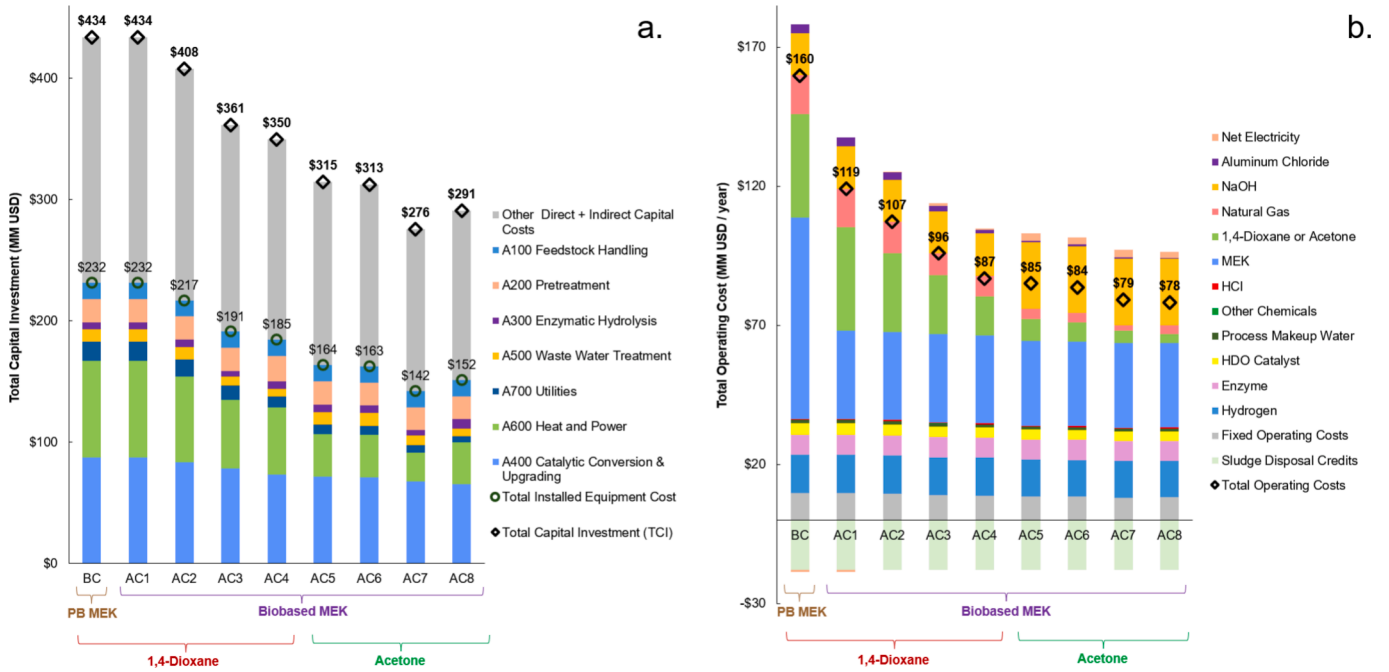

Fig. 5. (a) Total Capital Investment for the base case and alternative cases 1 through 8 (diamonds), Total Installed Equipment Cost (circles), and share distribution of process areas (stacked columns). (b) Annual Total Operating Cost for the base case and alternative cases 1 through 8 (diamonds) and share distribution of variable and fixed costs and credits (stacked columns). Note that Other Direct + Indirect Capital Costs are dependent on the TIEC.

(boiling point 56 °C), minimal water recirculation, and repositioned distillation unit significantly reduce heat demand, particularly in the solvent recovery step, allowing for smaller boilers, more compact equipment, and lower natural gas consumption compared to 1,4-dioxane systems. In 1,4-dioxane systems, the distilled solvent stream carries high water content (~20 wt%, boiling point 87 °C), which increases heat waste and requires additional solvent makeup to offset dilution caused by water in the recirculation loop. This leads to higher mass flow in the distillation unit, increased solvent loss, larger A600 and A400 areas, and greater natural gas consumption.

Additional sodium hydroxide was required in acetone systems to raise the initial pH to 13.0 during the aldol-condensation step, increasing NaOH's contribution to the TOC and partially offsetting the benefits of solvent replacement (Fig. 5**b**). Unlike the MFSP trend in cases 3 and 4, in case 8, the higher installed cost of areas A600 and A300 (after including the evaporation system) outweighed the TOC reduction from acetone's lower annual cost compared to case 7. A power surplus was identified for the base case and alternative case 1 (Fig. 4, Fig. 5**b**, and Table 3), as the heat demand required sufficient steam production for extra electricity generation. Paper sludge disposal credits (costs that companies incur for trucking and landing paper sludge) were included in all cases, and no SAF credits were considered, consistent with the previously published life-cycle assessment [66]. The reduction in the contribution to the MFSP of natural gas across the analyzed scenarios is offset by the increase in the cost of electricity acquired from the grid, as the steam turbine generator operates with enough steam to supply the heat demand of the biorefinery after crossing adequate hot and cold streams using heat exchangers (*Supplementary material, S18*).

Alternative case 7 achieved the lowest MFSP at $4.5/GGE, 48 % below the base case and 35 % below alternative case 1. In contrast, NREL estimated the MFSP of biomass-derived hydrocarbon products in the jet fuel range at $5.51/GGE (hydroprocessed esters and fatty acids from used cooking oil), $4.71/GGE (Ethanol-to-jet from corn), and $4.66/GGE (Fischer-Tropsch from forest residue) [67–69]. While biobased MEK and alternative solvent strategies can reduce the MFSP of the hydrocarbon blend from paper sludge, the estimated MFSP still exceeds the conventional gasoline price of $2.49/gal (U.S. Gulf Coast, 2023) [70]. However, this analysis suggests that replacing 1,4-dioxane with acetone in sugar dehydration is a promising approach that can contribute to developing cost-effective hydrocarbon production from lignocellulosic biomass via catalytic upgrading of furans.

3.13. Sensitivity assessment

The sensitivity assessment results for the base case and alternative cases 1 and 7 are shown in Fig. 6. In Fig. 6**a** and Fig. 6**b**, the top five variables influencing the base case MFSP are fiber consistency during hydrolysis, solvent loss, Internal Rate of Return (IRR), organic solvent-to-aqueous volume ratio (dehydration step), and petroleum-based MEK price. In alternative case 1 (Fig. 5**c** and Fig. 5**d**), nearly the same parameters apply, except MEK price, which is replaced by price of 1,4-dioxane, as the price of MEK is reduced in this scenario (biobased MEK). As previously described, fiber consistency for enzymatic hydrolysis indirectly impacts parameters related to the organic solvent in the dehydration reaction, meaning that in the base case and alternative case 1, three to four of the top five variables are intrinsically related to the solvent system used. In contrast, replacing 1,4-dioxane with acetone (alternative cases 5 to 8) shifts the key influencing variables. As shown in Fig. 6**e** and Fig. 6**f**. After upgrading the solvent system, other optimizable variables, such as the prices of biobased MEK and NaOH, 5-HMF yield, NaOH loading in aldol condensation, and enzyme loading, become most relevant for further MFSP reduction. These results suggest that improving economic viability of the proposed process requires further research on critical areas, including the integration of recyclable aldol-condensation catalysts (e.g., solid catalysts), the identification of more cost-effective biobased MEK production methods, the study of dehydration catalysts that improve the yields of 5-HMF and furfural in acetone systems, and the study of strategies for enzymatic hydrolysis at higher fiber consistency (e.g., >30 wt%), etc.

4. Conclusions

Carbohydrates from paper sludge were successfully converted into a hydrocarbon blend, predominantly in the C_9-C_{10} range, consisting of n-

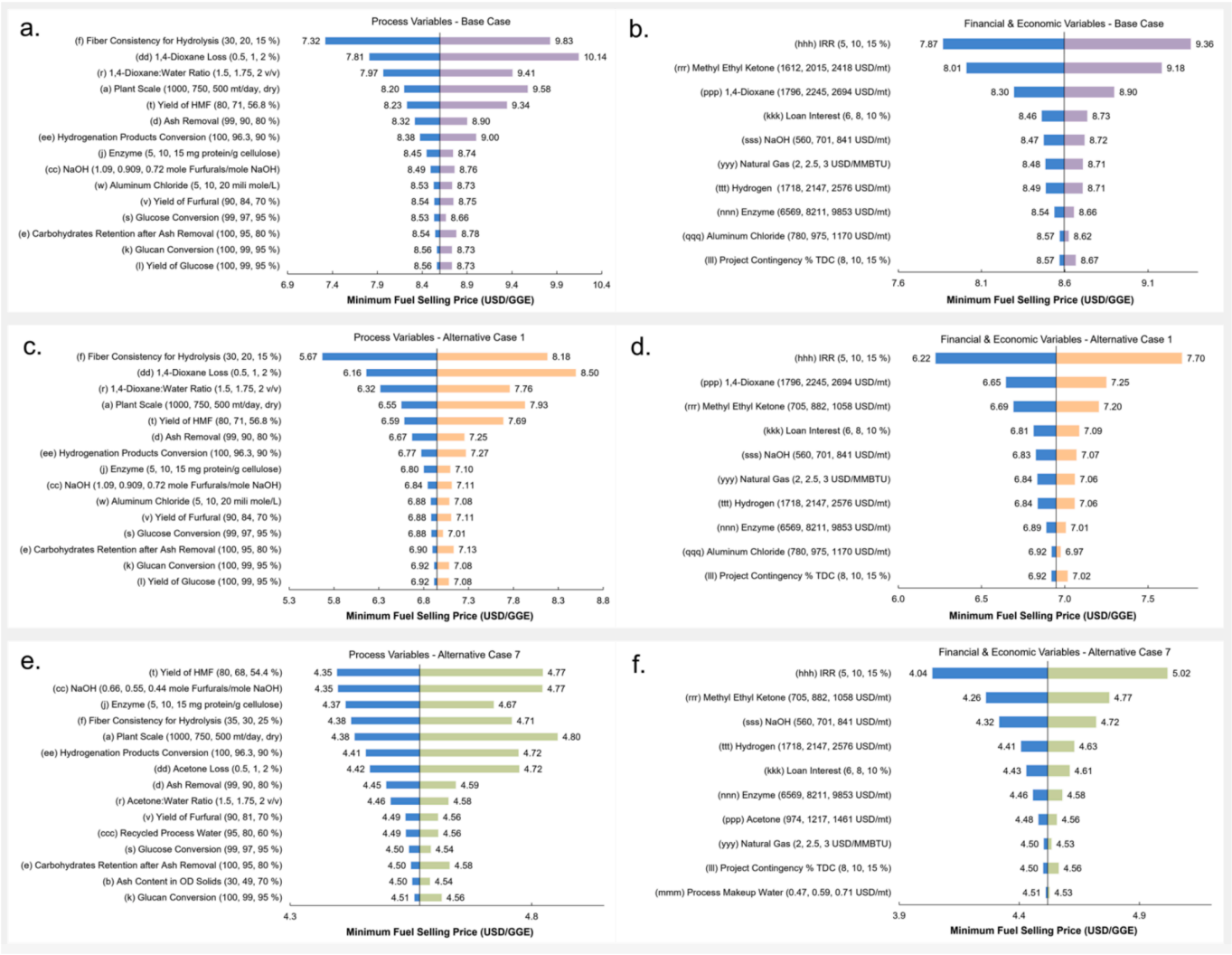

Fig. 6. Sensitivity assessment results displaying the primary operational, financial & economic variables affecting the MFSP of the hydrocarbon product derived from paper sludge in the base case (a & b), alternative case 1 (c & d), and alternative case 7 (e & f).

alkanes, *iso*-alkanes, and cycloalkanes. Notably, 44.3 % of the hydrocarbon product falls within the Jet A boiling range (156 °C – 293 °C), making this fraction suitable for blending into jet fuel. This cut meets the most critical ASTM specifications for Jet A, as confirmed by two independent fuel property testing laboratories. The results of techno-economic and sensitivity assessments highlight the significant impact of replacing 1,4-dioxane with acetone in the sugar dehydration step and identify critical process optimization opportunities to further reduce the MFSP to economically competitive levels.

CRediT authorship contribution statement

David Cruz: Writing – review & editing, Writing – original draft, Visualization, Software, Methodology, Investigation, Formal analysis, Data curation, Conceptualization. **Hyeonji Park:** Writing – review & editing, Methodology, Investigation, Formal analysis, Data curation, Conceptualization. **Phoenix Tiller:** Writing – review & editing, Methodology, Investigation, Formal analysis, Data curation, Conceptualization. **Adarsh Kumar:** Writing – review & editing, Methodology, Investigation, Formal analysis, Data curation. **Ronalds Gonzalez:** Writing – review & editing, Supervision, Methodology, Formal analysis, Conceptualization. **Ashutosh Mittal:** Writing – review & editing, Validation, Methodology, Investigation, Formal analysis, Data curation, Conceptualization. **David K. Johnson:** Writing – review & editing, Validation, Supervision, Resources, Project administration, Methodology, Investigation, Formal analysis, Data curation, Conceptualization. **Sunkyu Park:** Writing – review & editing, Supervision, Resources, Project administration, Methodology, Investigation, Funding acquisition, Formal analysis, Conceptualization.

Declaration of competing interest

The authors declare that they have no known competing financial interests or personal relationships that could have appeared to influence the work reported in this paper.

Acknowledgments

The authors gratefully acknowledge the support provided by the U.S. Department of Energy's Bioenergy Technologies Office (BETO) under Award Number DE-EE0008498 for this research. We also extend sincere thanks to Dr. Robert McCormick (robert.mccormick@nrel.gov) and Dr. Gina Fioroni (gina.fioroni@nrel.gov) at the NREL Fuels and Combustion Science group, as well as Dr. Joshua Heyne (joshua.heyne@wsu.edu) and Dr. Harrison (Zhibin) Yang (zhibin.yang@wsu.edu) at the Bioproducts, Sciences, and Engineering Laboratory at Washington State University, for their fuel property analysis of the resulting hydrocarbon product derived from paper sludge. The views expressed herein do not

necessarily represent the views of the U.S. Department of Energy or the United States Government.

Appendix A. Supplementary material

Supplementary data to this article can be found online at https://doi.org/10.1016/j.cej.2025.160622.

Data availability

Data will be made available on request.

References

[1] B.C. Klein, B. Scheidemantle, R.J. Hanes, A.W. Bartling, N.J. Grundl, R.J. Clark, M. J. Biddy, L. Tao, C.T. Trinh, A.M. Guss, C.E. Wyman, A.J. Ragauskas, E.G. Webb, B. H. Davison, C.M. Cai, Economics and global warming potential of a commercial-scale delignifying biorefinery based on co-solvent enhanced lignocellulosic fractionation to produce alcohols, sustainable aviation fuels, and co-products from biomass, Energy Environ. Sci. 17 (2023) 1202–1215, https://doi.org/10.1039/d3ee02532b.

[2] United Nations, Kyoto Protocol to the United Nations Framework Convention on Climate Change, 1998. https://unfccc.int/resource/docs/convkp/kpeng.pdf.

[3] K. Morganti, K. Moljord, R. Pearson, M. Vermeire, M. Traver, P. Scorletti, T. de Melo, Y. Wang, P. China, J. Repasky, F. Oliva, A. Bason, Low carbon transportation fuels: deployment pathways, opportunities and challenges, Energy Environ. Sci. 17 (2023) 531–568, https://doi.org/10.1039/d3ee01328f.

[4] M.J. Pickl, The renewable energy strategies of oil majors – from oil to energy? Energy Strateg. Rev. 26 (2019) https://doi.org/10.1016/j.esr.2019.100370.

[5] N. Shakelly, Z. Li, S. Deng, J.W. Sutherland, Effect of key economic uncertainties on the techno-economic performance of the production of high energy-content jet fuel blending components derived from bio-ethanol, Sustain. Energy Technol. Assess. 65 (2024), https://doi.org/10.1016/j.seta.2024.103747.

[6] S.M. Katalenich, M.Z. Jacobson, Toward battery electric and hydrogen fuel cell military vehicles for land, air, and sea, Energy 254 (2022) 124355, https://doi.org/10.1016/j.energy.2022.124355.

[7] U.S. Environmental Protection Agency, Fast Facts U.S. Transportation Sector Greenhouse Gas Emissions 1990-2022, 2024. https://epa.gov.

[8] U.S. Environmental Protection Agency, Inventory of U.S. Greenhouse Gas Emissions and Sinks, 2024. https://www.epa.gov.

[9] U.S. Department of Energy, U.S. Department of Transportation, U.S. Department of Agriculture, Memorandum of Understanding Sustainable Aviation Fuel Grand Challenge, 2021. https://www.energy.gov.

[10] U.S. Department of Energy, U.S. Department of Agriculture, U.S. Department of Transportation, U.S. Environmental Protection Agency, SAF Grand Challenge Roadmap, 2022. https://www.energy.gov.

[11] ASTM International, ASTM D7566-24b Standard Specification for Aviation Turbine Fuel Containing Synthesized Hydrocarbons, 2024. https://doi.org/10.1520/D7566.

[12] National Renewable Energy Laboratory, U.S. Airport Infrastructure and Sustainable Aviation Fuel, 2021.

[13] U.S. Department of Energy, Sustainable Aviation Fuel Review of Technical Pathways, 2020. https://www.energy.gov/sites/prod/files/2020/09/f78/beto-sust-aviation-fuel-sep-2020.pdf.

[14] B.W. Kolosz, Y. Luo, B. Xu, M.M. Maroto-Valer, J.M. Andresen, Life cycle environmental analysis of "drop in" alternative aviation fuels: a review, Sustain. Energy Fuels 4 (2020) 3229–3263, https://doi.org/10.1039/c9se00788a.

[15] National Renewable Energy Laboratory, Sustainable Aviation Fuel (SAF) State-of-Industry Report : State of SAF Production Process, 2024. https://www.nrel.gov.

[16] U.S. Government Accountability Office, Sustainable Aviation Fuel - Agencies Should Track Progress toward Ambitious Federal Goals, 2023. https://www.gao.gov.

[17] D. Lebedeva, L.W. Schick, D. Cracco, W. Sangsuwan, G. Castiella-Ona, D.O. Silva, A. Marson, E. Svensson Grape, A.K. Inge, L.M. Rossi, E. Subbotina, A. Manzardo, J. S.M. Samec, Sustainable aviation fuel from prehydrolysis liquors, Green Chem. 26 (2024) 7258–7267, https://doi.org/10.1039/d4gc01257g.

[18] N.R. Baral, O. Kavvada, D. Mendez-Perez, A. Mukhopadhyay, T.S. Lee, B. A. Simmons, C.D. Scown, Techno-economic analysis and life-cycle greenhouse gas mitigation cost of five routes to bio-jet fuel blendstocks, Energy Environ. Sci. 12 (2019) 807–824, https://doi.org/10.1039/c8ee03266a.

[19] J. Slak, B. Pomeroy, A. Kostyniuk, M. Grilc, B. Likozar, A review of bio-refining process intensification in catalytic conversion reactions, separations and purifications of hydroxymethylfurfural (HMF) and furfural, Chem. Eng. J. 429 (2022), https://doi.org/10.1016/j.cej.2021.132325.

[20] B. Klein, I. McNamara, R. Davis, A. Mittal, D. Johnson, Techno-Economic Assessment for the Production of Hydrocarbon Fuels via Catalytic Upgrading of Furans - NREL/TP-5100-80652, 2021. https://www.nrel.gov.

[21] G.W. Huber, J.N. Chheda, C.J. Barrett, J.A. Dumesic, Production of Liquid Alkanes by Aqueous-Phase Processing of Biomass-Derived Carbohydrates, Science (80-.). 308 (2005) 1446–1450. https://doi.org/10.1126/science.1111166.

[22] U.S. Department of Energy, Top Value Added Chemicals from Biomass Volume I, 2004. https://doi.org/10.2172/15008859.

[23] J. Zhang, X. Wang, B. Yang, X. Zeng, Q. Zhang, J.J. Zou, J. Xie, Superhydrophobic and superacid magnetic catalyst induced highly selective aldol condensation and alkylation for high-density biofuels, Fuel 378 (2024) 1–8, https://doi.org/10.1016/j.fuel.2024.132930.

[24] A.J. Foster, P.T.M. Do, R.F. Lobo, The synergy of the support acid function and the metal function in the catalytic hydrodeoxygenation of m-cresol, Top. Catal. 55 (2012) 118–128, https://doi.org/10.1007/s11244-012-9781-7.

[25] H. Ren, W. Yu, M. Salciccioli, Y. Chen, Y. Huang, K. Xiong, D.G. Vlachos, J.G. Chen, Selective hydrodeoxygenation of biomass-derived oxygenates to unsaturated hydrocarbons using molybdenum carbide catalysts, ChemSusChem 6 (2013) 798–801, https://doi.org/10.1002/cssc.201200991.

[26] American Forest & Paper Association, AF & PA Details US Paper Production and Capacity Trends, (2024).

[27] T. Zhang, Á.G. Rivas, X.F. Fernandez, N. Li, E. Gucho, L. Zhu, A. Bijl, J.L. Llacuna, S. He, Fast pyrolysis of paper sludge in a continuous stirred-tank reactor and liquid-liquid extraction of benzenoid aromatics from fast pyrolysis bio-liquid, Renew. Energy 236 (2024) 1–8, https://doi.org/10.1016/j.renene.2024.121429.

[28] C.V.T. Mendes, J.M.S. Rocha, M.G.V.S. Carvalho, Valorization of residual streams from pulp and paper mills: pretreatment and bioconversion of primary sludge to bioethanol, Ind. Eng. Chem. Res. 53 (2014) 19398–19404, https://doi.org/10.1021/ie503021y.

[29] A. Sluiter, B. Hames, R. Ruiz, C. Scarlata, J. Sluiter, D. Templeton, D. Crocker, Determination of structural carbohydrates and lignin in Biomass - NREL/TP-510-42618, 2012. http://www.nrel.gov.

[30] A. Sluiter, B. Hames, D. Hyman, C. Payne, R. Ruiz, C. Scarlata, J. Sluiter, D. Templeton, J.W. Nrel, Determination of total solids in biomass and total dissolved solids in liquid process samples - NREL/TP-510-42621, 2008. http://www.nrel.gov.

[31] A. Sluiter, B. Hames, R. Ruiz, C. Scarlata, J. Sluiter, D. Templeton, Determination of Ash in Biomass - NREL/TP-510-42622, 2008. https://www.nrel.gov.

[32] H. Park, D. Cruz, P. Tiller, D.K. Johnson, A. Mittal, H. Jameel, R. Venditti, S. Park, Effect of ash in paper sludge on enzymatic hydrolysis, Biomass Bioenergy 165 (2022) 106567, https://doi.org/10.1016/j.biombioe.2022.106567.

[33] A. Mittal, H.M. Pilath, D.K. Johnson, Direct conversion of biomass carbohydrates to platform chemicals: 5-Hydroxymethylfurfural (HMF) and furfural, Energy Fuel 34 (2020) 3284–3293, https://doi.org/10.1021/acs.energyfuels.9b04047.

[34] ASTM International, ASTM D2887-23 Standard Test Method for Boiling Range Distribution of Petroleum Fractions by Gas Chromatography, 2023. https://doi.org/10.1520/mnl10902m.

[35] ASTM International, ASTM D5972-23 Standard Test Method for Freezing Point of Aviation Fuels, 2023. https://doi.org/10.1520/mnl10883m.

[36] ASTM International, ASTM D6450-16a Standard Test Method for Flash Point by Modified Continuously Closed Cup, 2021. https://doi.org/10.1520/D6450-16AR21.2.

[37] J. Heyne, B. Rauch, P. Le Clercq, M. Colket, Sustainable aviation fuel prescreening tools and procedures, Fuel 290 (2021) 120004, https://doi.org/10.1016/j.fuel.2020.120004.

[38] R. Davis, N. Grundl, L. Tao, M.J. Biddy, E.C.D. Tan, G.T. Beckham, D. Humbird, D. N. Thompson, M.S. Roni, Process Design and Economics for the Conversion of Lignocellulosic Biomass to Hydrocarbon Fuels and Coproducts: 2018 Biochemical Design Case Update, 2018. https://www.nrel.gov.

[39] R. Davis, L. Tao, C. Scarlata, E.C.D. Tan, J. Ross, J. Lukas, D. Sexton, Process Design and Economics for the Conversion of Lignocellulosic Biomass to Hydrocarbons: Dilute-Acid and Enzymatic Deconstruction of Biomass to Sugars and Catalytic Conversion of Sugars to Hydrocarbons, 2015. https://www.nrel.gov.

[40] Economic Indicators Chem. Eng., Chem. Eng. 131 (2024). https://www.chemengonline.com/.

[41] P. Tiller, H. Park, D. Cruz, E. Carrejo, D.K. Johnson, A. Mittal, R. Venditti, S. Park, Techno-economic analysis of biomass value-added processing informed by pilot scale de-ashing of paper sludge feedstock, Bioresour. Technol. 401 (2024) 130744, https://doi.org/10.1016/j.biortech.2024.130744.

[42] L. Wang, R. Templer, R.J. Murphy, High-solids loading enzymatic hydrolysis of waste papers for biofuel production, Appl. Energy 99 (2012) 23–31, https://doi.org/10.1016/j.apenergy.2012.03.045.

[43] J. Esteban, A.J. Vorholt, W. Leitner, An overview of the biphasic dehydration of sugars to 5-hydroxymethylfurfural and furfural: a rational selection of solvents using COSMO-RS and selection guides, Green Chem. 22 (2020) 2097–2128, https://doi.org/10.1039/c9gc04208c.

[44] Y. Kim, A. Mittal, D.J. Robichaud, H.M. Pilath, B.D. Etz, P.C. St, D.K. John, S. K. Johnson, Prediction of hydroxymethylfurfural yield in glucose conversion through investigation of lewis acid and organic solvent effects, ACS Catal. 10 (2020) 14707–14721, https://doi.org/10.1021/acscatal.0c04245.

[45] M. Hichri, R. Besbes, Z. Trasbelsi, N. Ouerfelli, I. Khattech, Isobaric vapour–liquid phase diagram and excess properties for the binary system 1,4-dioxane + water at 298.15 K, 318.15 K and 338.15 K, Phys. Chem. Liq. 52 (2014) 373–387, https://doi.org/10.1080/00319104.2013.833618.

[46] H. Xin, T. Zhang, W. Li, M. Su, S. Li, Q. Shao, L. Ma, Dehydration of glucose to 5-hydroxymethylfurfural and 5-ethoxymethylfurfural by combining Lewis and Brønsted acid, RSC Adv. 7 (2017) 41546–41551, https://doi.org/10.1039/c7ra07684c.

[47] H. Zhu, Y. Zhang, X. Guo, Y. Cheng, L. Wang, X. Li, Efficient one-pot production of 5-hydroxymethylfurfural from glucose in an acetone-water solvent, Ind. Eng. Chem. Res. 61 (2022) 5661–5671, https://doi.org/10.1021/acs.iecr.2c00502.

[48] A. Farooq, S. Shuing Lam, J. Jae, M. Ali Khan, B.H. Jeon, S.C. Jung, Y.K. Park, Jet fuel-range hydrocarbons generation from the pyrolysis of saw dust over Fe and Mo-

loaded HZSM-5(38) catalysts, Fuel 333 (2023), https://doi.org/10.1016/j.fuel.2022.126313.
[49] X. Cui, X. Zhao, D. Liu, A novel route for the flexible preparation of hydrocarbon jet fuels from biomass-based platform chemicals: a case of using furfural and 2,3-butanediol as feedstocks, Green Chem. 20 (2018) 2018–2026, https://doi.org/10.1039/c8gc00292d.
[50] A. Tampieri, C. Russo, R. Marotta, M. Constantí, S. Contreras, F. Medina, Microwave-assisted condensation of bio-based hydroxymethylfurfural and acetone over recyclable hydrotalcite-related materials, Appl. Catal. B Environ. 282 (2021) 1–12, https://doi.org/10.1016/j.apcatb.2020.119599.
[51] G. Morales, M. Paniagua, D. de la Flor, M. Sanz, P. Leo, C. López-Aguado, H. Hernando, S.A. Orr, K. Wilson, A.F. Lee, J.A. Melero, Aldol condensation of furfural and methyl isobutyl ketone over Zr-MOF-808/silica hybrid catalysts, Fuel 339 (2023) 8, https://doi.org/10.1016/j.fuel.2023.127465.
[52] R.S. Malkar, H. Daly, C. Hardacre, G.D. Yadav, Aldol condensation of 5-hydroxymethylfurfural to fuel precursor over novel aluminum exchanged-DTP@ZIF-8, ACS Sustain. Chem. Eng. 7 (2019) 16215–16224, https://doi.org/10.1021/acssuschemeng.9b02939.
[53] C.R. Waidmann, A.W. Pierpont, E.R. Batista, J.C. Gordon, R.L. Martin, L.A. Pete Silks, R.M. West, R. Wu, Functional group dependence of the acid catalyzed ring opening of biomass derived furan rings: an experimental and theoretical study, Catal. Sci. Technol. 3 (2013) 106–115, https://doi.org/10.1039/c2cy20395b.
[54] X. Li, J. Sun, S. Shao, X. Hu, Y. Cai, Aldol condensation/hydrogenation for jet fuel from biomass-derived ketone platform compound in one pot, Fuel Process. Technol. 215 (2021), https://doi.org/10.1016/j.fuproc.2021.106768.
[55] A.D. Sutton, F.D. Waldie, R. Wu, M. Schlaf, L.A. 'Pete'Silks, J.C. Gordon, The hydrodeoxygenation of bioderived furans into alkanes, Nat. Chem. 5 (2013) 428–432. https://doi.org/10.1038/nchem.1609.
[56] T. Prasomsri, T. Nimmanwudipong, Y. Román-Leshkov, Effective hydrodeoxygenation of biomass-derived oxygenates into unsaturated hydrocarbons by MoO3 using low H2 pressures, Energy Environ. Sci. 6 (2013) 1732–1738, https://doi.org/10.1039/c3ee24360e.
[57] J. Yang, Z. Xin, Q. (Sophia) He, K. Corscadden, H. Niu, An overview on performance characteristics of bio-jet fuels, Fuel 237 (2019) 916–936. https://doi.org/10.1016/j.fuel.2018.10.079.
[58] FisherSolve, FisherSolve Next, (2024) 1–2. https://www.fishersolve.net (accessed October 5, 2024).
[59] M. Kato, H. Konishi, M. Hirata, Apparatus for measurement of isobaric dew and bubble points and vapor-liquid equilibria methanol-water and water-dioxane systems, J. Chem. Eng. Data 15 (1970) 501–505, https://doi.org/10.1021/je60047a022.
[60] J. Polednová, I. Wichterle, Vapour-liquid equilibrium in the acetone-water system at 101.325kPa, Fluid Phase Equilib. 17 (1984) 115–121, https://doi.org/10.1016/0378-3812(84)80015-1.
[61] F. Gu, Y. Hou, Salt effects on the isobaric vapor-liquid equilibrium for four binary systems, J. Chem. Eng. Data 45 (2000) 467–470, https://doi.org/10.1021/je990215s.
[62] C.A.S. Hall, B.E. Dale, D. Pimentel, Seeking to understand the reasons for different energy return on investment (EROI) estimates for biofuels, Sustainability 3 (2011) 2413–2432, https://doi.org/10.3390/su3122413.
[63] R. Patnaik, N. Mallick, Microalgal biodiesel production: realizing the sustainability index, Front. Bioeng. Biotechnol. 9 (2021) 1–15, https://doi.org/10.3389/fbioe.2021.620777.
[64] G.M. Figueroa-Torres, C. Theodoropoulos, Techno-economic analysis of a microalgae-based biorefinery network for biofuels and value-added products, Bioresour. Technol. Reports 23 (2023) 101524, https://doi.org/10.1016/j.biteb.2023.101524.
[65] R. Piastrellini, A.P. Arena, B. Civit, Energy life-cycle analysis of soybean biodiesel: effects of tillage and water management, Energy 126 (2017) 13–20, https://doi.org/10.1016/j.energy.2017.03.028.
[66] K. Lan, D. Cruz, J. Li, A.A. Agyei Boakye, H. Park, P. Tiller, A. Mittal, D.K. Johnson, S. Park, Y. Yao, Life-cycle assessment of sustainable aviation fuel derived from paper sludge, ACS Sustain. Chem. Eng. 12 (2024) 8379–8390, https://doi.org/10.1021/acssuschemeng.4c00795.
[67] U.S. Department of Energy, 2022 Annual Technology Baseline / Aviation Fuels, (2022). https://atb.nrel.gov (accessed August 31, 2024).
[68] L. Tao, J.N. Markham, Z. Haq, M.J. Biddy, Techno-economic analysis for upgrading the biomass-derived ethanol-to-jet blendstocks, Green Chem. 19 (2017) 1082–1101, https://doi.org/10.1039/c6gc02800d.
[69] E.C.D. Tan, L.J. Snowden-Swan, M. Talmadge, A. Dutta, S. Jones, K.K. Ramasamy, M. Gray, R. Dagle, A. Padmaperuma, M. Gerber, A.H. Sahir, L. Tao, Y. Zhang, Comparative techno-economic analysis and process design for indirect liquefaction pathways to distillate-range fuels via biomass-derived oxygenated intermediates upgrading, Biofuels Bioprod. Biorefining 11 (2017) 41–66, https://doi.org/10.1002/bbb.1710.
[70] U.S. Energy Information Administration, Petroleum & Other Liquids / U.S. Gulf Coast Kerosene-Type Jet Fuel Spot Price FOB, (2024). https://www.eia.gov (accessed August 31, 2024).
[71] U.S. Department of the Treasury, U.S. Internal Revenue Service, How To Depreciate Property, 2024. http://www.irs.gov.
[72] Federal Reserve Bank of St. Louis, Producer Price Index by Industry: Chemical Manufacturing, Fed. Reserv. Econ. Data (2024). https://fred.stlouisfed.org/.
[73] United States Department of Labor, Labor Index: Chemical Manufacturing, U.S. Bur. Labor Stat. Data (2024). https://www.bls.gov/.
[74] ICIS, Americas Chemical Outlook 2019, 2019.
[75] G. Zang, A. Shah, C. Wan, Techno-economic analysis of co-production of 2,3-butanediol, furfural, and technical lignin via biomass processing based on deep eutectic solvent pretreatment, Biofuels Bioprod. Biorefining 14 (2020) 326–343, https://doi.org/10.1002/bbb.2081.
[76] U.S. Energy Information Administration, Henry Hub Natural Gas Spot Price, (n.d.). https://www.eia.gov (accessed October 4, 2024).
[77] G.M. Scott, S. Abubakr, A. Smith, Sludge characteristics and disposal alternatives for the pulp and paper industry, 1995. https://www.tappi.org.
[78] V. Kumar, P. Verma, Pulp-paper industry sludge waste biorefinery for sustainable energy and value-added products development: a systematic valorization towards waste management, J. Environ. Manage. 352 (2024), https://doi.org/10.1016/j.jenvman.2024.120052.
[79] U.S. Energy Information Administration, Average retail price of electricity / Industrial / Annual, (2024). https://www.eia.gov (accessed April 10, 2024).
[80] S. Liu, Y. Zhu, Y. Liao, H. Wang, Q. Liu, L. Ma, C. Wang, Advances in understanding the humins: formation, prevention and application, Appl. Energy Combust. Sci. 10 (2022), https://doi.org/10.1016/j.jaecs.2022.100062.